In vivo staging of pathology in REM Sleep Behavior Disorder – a multi-modality imaging case-control study

Karoline Knudsen, PhD[1#], Tatyana D Fedorova, BSc[1#], Allan K Hansen, MD[1], Michael Sommerauer, MD[1,2], Marit Otto, PhD[3,4], Kristina B Svendsen, PhD[4], Adjmal Nahimi, PhD[1], Morten G Stokholm, PhD[1], Nicola Pavese, PhD[1,5,6], Christoph P Beier, MD[7], David J Brooks, DSc[1,5,6], and Per Borghammer, DMSc[1]*

[#] These authors contributed equally to the study.

[1]Aarhus University Hospital, Department of Nuclear Medicine and PET Centre, Aarhus, Denmark

[2]Department of Neurology, University Hospital Cologne, Cologne, Germany

[3]Aarhus University Hospital, Department of Clinical Neurophysiology, Aarhus, Denmark

[4]Aarhus University Hospital, Department of Neurology, Aarhus, Denmark

[5]Division of Neuroscience, Department of Medicine, Imperial College London, London, UK

[6]Division of Neuroscience, Newcastle University, Newcastle, UK

[7]Southern University of Denmark, Department of Neurology, Odense, Denmark

*Corresponding author: Per Borghammer, MD, PhD, DMSc
Email: perborgh@rm.dk
Phone: (+0045) 28261039
Fax: (+0045) 78463020
Department of Nuclear Medicine and PET Centre
Aarhus University Hospital
Nørrebrogade 44, Building 10G
8000 Aarhus C, Denmark

Word count:	Abstract:	429
	Manuscript:	3,833
	Figures / tables:	5 / 1
	References:	45

Keywords: REM sleep behaviour disorder, PET, MRI, F-DOPA, MIBG, donepezil, Parkinson

Running title: In vivo staging of neuropathology in iRBD

Abstract

Background. Accumulating evidence suggests that α-synuclein aggregates, a defining pathology of Parkinson's disease (PD), display cell-to-cell transmission. The initial α-synuclein aggregation may start in autonomic nerve terminals years prior to appearance of motor symptoms, and subsequently spread via autonomic nerves to the spinal cord and brainstem. If this hypothesis is correct, patients with idiopathic REM sleep behaviour disorder (iRBD), a prodromal phenotype of PD with RBD and dementia with Lewy bodies, could display a pattern of pathology where the peripheral autonomic nervous system and locus coeruleus (LC) are affected ahead of the nigrostriatal dopamine system. We aimed to investigate function of sympathetic, parasympathetic, noradrenergic, and dopaminergic innervation in iRBD patients using multi-modality imaging.

Methods. In this clinically prospective, case-control study, polysomnography-confirmed iRBD subjects without clinical signs of parkinsonism or dementia were recruited via advertisement and sleep clinics in Denmark. We used ^{11}C-donepezil PET/CT to assess their cholinergic activity (parasympathetic) in the gut, ^{123}I-MIBG scintigraphy to measure cardiac sympathetic function, neuromelanin-sensitive MRI to measure density of pigmented neurons of the LC, ^{11}C-MeNER PET to assess noradrenergic transporter availability in terminals originating from the LC, and ^{18}F-DOPA PET to assess nigrostriatal dopamine storage capacity. For each imaging modality, findings for iRBD subjects were compared to those of controls without neurological disorders or cognitive impairment and to symptomatic PD patients. Imaging data were interrogated with one-way ANOVAs corrected for multiple comparisons.

Findings. Twenty two iRBD patients were consecutively included between June 2016 and Dec 2017. Compared to healthy controls, the iRBD patients showed significant decreases in colonic ^{11}C-donepezil uptake (-0·322 (CI-0·112; -0·531); p=0·0020), ^{123}I-MIBG heart-mediastinum ratios (-0·508 (CI:-0·353; -0·664); p<0·0001), neuromelanin-MRI LC/pons ratios (-0·059 (CI:-0·019; -0·099); p=0·0028), ^{11}C-MeNER binding potential in the left thalamus (-0·080 (CI:-0·010; -0·150) p=0·023), and putaminal ^{18}F-DOPA Ki (-0·0023 (CI:-0·0009; -0·0037); p=0·0013). The iRBD and PD groups had similar gut ^{11}C-donepezil (p=0·39), heart ^{123}I-MIBG (p>0·99), neuromelanin-MRI (P=0·96), and brain ^{11}C-MeNER signals (P=0·66). In contrast, while 71% of iRBD cases had normal putamen ^{18}F-FDOPA Ki values, this was significantly reduced in all the PD patients (iRBD vs. PD: p<0·0001).

2

Interpretation.

Patients with iRBD displayed similar peripheral dysfunction to symptomatic PD in their sympathetic and parasympathetic nervous systems, and a similar loss of pigmented cells of the LC. In contrast to PD, 71% of iRBD cases had normal putaminal dopaminergic storage capacity. As iRBD can progress to PD with RBD or DLB, the peripheral dysfunction present in the absence of dopamine terminal damage supports the hypothesis that α-synuclein pathology in PD targets peripheral autonomic nerves ahead of involving nigral cells in the midbrain.

Research in context

Background

Prospective studies have shown that most cases of idiopathic rapid-eye-movement sleep behaviour disorder (iRBD) represents a prodromal phenotype of the synucleinopathies Parkinson's disease (PD) or dementia with Lewy bodies (DLB). We searched PubMed in all languages on December 20, 2017 using the keywords "Parkinson disease", "Lewy body disease", "REM sleep behaviour disorder", "positron-emission tomography", "tomography emission-computed single-photon", "magnetic resonance imaging", "dual-hit hypothesis", "alpha-synuclein". We found no previous *in vivo* studies which had used multimodal imaging to comprehensively assess the levels of dysfunction in the autonomic nervous system, locus coeruleus, and substantia nigra of patients with iRBD or genetically susceptible prodromal PD cohorts.

Accumulating evidence suggests that the defining pathology of PD, aggregated α-synuclein, is capable of cell-to-cell transmission. It has been hypothesised that the initial misfolding and aggregation may occur in the olfactory bulb and autonomic nerve terminals, and then spread centripetally to the brain. This view is supported by evidence that peripheral-to-central spreading of α-synuclein can be induced in animal models, by epidemiological evidence that total vagotomy protects against PD, and the finding of pathological α-synuclein aggregates in the gut of PD patients years prior to their diagnosis.

Added value of this study

To our knowledge, we present the most comprehensive imaging study to date of iRBD, potentially a prodromal PD+RBD/DLB patient cohort. We demonstrate convincing sympathetic and parasympathetic dysfunction in iRBD patients equivalent to that seen in diagnosed PD patients, along with similar loss of pigmented locus coeruleus cells and thalamic noradrenaline transporters. In contrast to PD patients, 71% of our iRBD cases had normal ^{18}F-FDOPA uptake in their putamen.

Implications

Our imaging findings support the hypothesis that those PD cases with RBD have early dysfunction in their peripheral autonomic system and locus coeruleus prior to involvement of their nigral dopamine system by α-synuclein pathology.

4

Introduction

The pathological hallmarks of Parkinson's disease (PD) are progressive loss of nigrostriatal dopaminergic innervation and the presence of abnormal α-synuclein (α-syn) aggregates in vulnerable neuron populations. Accumulating evidence suggests that misfolded α-syn protein can act as a template, encouraging further α-syn to misfold with formation of insoluble filamentous inclusions which are capable of cell-to-cell transmission through interconnected neuronal pathways[1]. In most cases of PD, the distribution of brain α-syn inclusions displays a characteristic caudo-rostral gradient with the lower brainstem nuclei becoming first involved[2]. It has been hypothesized that α-syn aggregates initially form in the olfactory bulb and nerve terminals of the gastrointestinal lining. Subsequently, the pathology spreads via autonomic nerves to the dorsal motor nucleus of the vagus (DMV) and intermediolateral cell columns (IML) of the sympathetic system[3,4]. This hypothesis is supported by animal studies showing that peripheral-to-central spreading of α-syn aggregates through autonomic nerves can be induced[5], epidemiological evidence that truncal vagotomy is protective against PD[6,7], and the finding of α-syn inclusions in gastrointestinal nerve fibres many years prior to clinical PD diagnosis[8]. However, human autopsies have failed to support the view that PD is initiated in the gut[9]. Currently, cell-to-cell transmission of aggregated α-syn and the peripheral-onset hypothesis are intensely debated topics in PD research[4,10,11].

In the present study, we performed comprehensive multimodal imaging of patients with idiopathic rapid-eye-movement sleep behaviour disorder (iRBD). Most iRBD cases will eventually develop a synucleinopathy – PD with RBD, dementia with Lewy bodies (DLB), or rarely, multiple system atrophy (MSA)[12,13]. iRBD is believed to arise from degeneration of the pontine nuclei, including the magnocellular reticular formation, sublaterodorsal nucleus, and peri-coeruleus complex[2,14]. These structures are situated close to the locus coeruleus (LC). Importantly, pathological phosphorylated α-syn inclusions have been detected in the colon and sympathetic chain in iRBD patients[15,16]. If the peripheral-to-central spreading hypothesis of α-syn is correct, we predicted that a significant fraction of iRBD cases would display dysfunction of peripheral autonomic nerves equivalent to that seen in symptomatic PD, and that the LC could be involved ahead of the dopamine cells in the substantia nigra compacta which would be relatively spared as iRBD patients do not exhibit overt parkinsonism. We used ^{11}C-donepezil PET-CT to assess

5

cholinergic (including parasympathetic) activity of the gut[17,18], ^{123}I-MIBG scintigraphy to measure integrity of sympathetic cardiac innervation[19], neuromelanin-sensitive MRI to measure the density of pigmented cell bodies of the LC[20,21], ^{11}C-MeNER PET to assess thalamic noradrenaline transporter binding in the terminals of LC projections[21,22], and finally ^{18}F-DOPA PET to assess nigrostriatal dopamine storage capacity[23].

Methods

Study design and participants

The study was conducted between June 3rd, 2016, and December 19th, 2017. We recruited consecutively 22 iRBD patients with polysomnographic confirmation (**Supplementary methods**). Inclusion criteria: iRBD diagnosis according to International Classification of Sleep Disorders III, age 50-85 years. Exclusion criteria: A clinical diagnosis of PD or DLB according to consensus criteria[24,25], a Montreal Cognitive assessment (MoCA) score <23, or the presence of psychiatric disorders, medication interfering with the noradrenergic system, cholinesterase inhibitors, diabetes, neuropathies, heart- or kidney failure, current or previous cancer and/or major surgery on abdominal organs, inflammatory bowel disease.

Table 1 summarizes clinical and demographic data of the iRBD patients and imaging-modality specific PD and control groups who were scanned with identical methodologies. More clinical information is listed in **Supplementary table 1**. Much of the reference imaging data has been published previously[17,21,23]. The study was approved by the Science Ethical Committee of the Central Denmark Region (case nr. 1-10-72-160-16). All subjects provided informed written consent according to the Declaration of Helsinki.

Imaging

The five imaging modalities and their relationship to neuropathological Braak stages I-III of α-syn aggregation in PD are represented in **Figure 1**. The sympathetic autonomic nuclei are not part of the original Braak PD staging scheme[2], but are included here in stage I as the IML and

paravertebral sympathetic chain are nearly always involved in cases with incidental Lewy body disease[26,27].

All subjects were scanned on either 3T Siemens TRIO or 3T Siemens SKYRA MR systems; protocols included T1 and fluid-attenuated inversion recovery images. Neuromelanin sensitive images were obtained in a subset of 11 iRBD patients, as previously described[21]. Using a volume of interest (VOI) approach, LC/pons ratios were calculated (**Supplementary methods**). All MRI and PET analyses were performed in PMOD 3·6 (*PMOD, Zürich, Switzerland*).

[11]C-donepezil PET/CT was performed, as previously described[17]. Subjects fasted for at least 8 hours and abstained from drinking 4 hours before PET. Forty-five minutes after injection of 500 MBq ^{11}C-donepezil, static PET images were performed in 3D-mode with the abdominal organs in field-of-view. High-resolution CT with contrast-enhancement was performed immediately prior to PET. Body-weight corrected standard uptake values (SUV) were calculated: SUV = concentration (kBq/mL)/[injected dose (kBq)/body weight (g)]. VOIs were defined on the small and large intestine as previously described[17]. Intra-luminal water content was excluded from the small intestine and SUVs were extracted from the VOIs. Small intestine and colon SUVs were adjusted for volume to avoid underestimating the PET signal in PD and iRBD patients[17].

^{123}I-MIBG scintigraphy was performed using a dual-head gamma camera (*Siemens Symbia SPECT/CT, Erlangen, Germany*) with a low-energy high-resolution collimator. 15-minute images of the thorax were obtained 15 minutes (early) and 3·5 hours (late) after injection of 110 MBq ^{123}I-MIBG. Regions of interest were defined on the heart and mediastinum. Mean heart-uptake /mean mediastinum-uptake (H/M) ratios were calculated on early and late images, and washout rates (WR) were calculated as $H/M_{late} - H/M_{early}$.

^{18}F-DOPA and ^{11}C-MeNER PET was performed, as previously described[21,23]. One hour before ^{18}F-FDOPA injection, 150 mg of carbidopa was administered orally. After a transmission scan, tracer doses of 120 MBq ^{18}F-DOPA or 550 MBq ^{11}C-MeNER were injected intravenously and dynamic PET (FDOPA 94·5 min; MeNER 90 min) acquired in list mode on an ECAT high-resolution research tomograph (HRRT; *Siemens/CTI, Knoxville, TN*). PET data were reconstructed using a 3D-OSEM algorithm yielding dynamic PET data volumes (**Supplementary methods**). PET images were normalized to MNI space with rigid matching of subject's PET to the anatomical MRI, and MRI segmentation using the built-in Hammers N30R83 atlas.

7

Table 1. Demographic and clinical data of the iRBD patients, and the PD and healthy control (HC) reference groups.

	Sex, m/f	Age, y	DD, y	UPDRS	H&Y I/II/III/IV	MMSE	MOCA	OH, y/n	Olfaction	NMSQuest
Donepezil										
RBD	16/4	68±9	-	1 (0-5)	-	-	27 (23-30)	7/13	6 (2-13)	7 (2-15)
PD	10/8	62±8	1·7±0·6	19 (6-26)	0/14/2/0	29 (27-30)	-	-	6 (1-14)	7 (2-14)
HC	9/7	65±6	-	-	-	29 (24-30)	-	-	11 (6-13)	1 (0-7)
MIBG										
RBD	18/4	68±9	-	1 (0-5)	-	-	27 (23-30)	7/15	6 (2-13)	7 (2-15)
PD	12/5	65±8	9.9±2.8	43 (25-52)	0/10/7/0	29 (24-30)	-	2/13	7 (2-11)	-
HC	4/6	63±9	-	-	-	30 (27-30)	-	0/6	11 (8-13)	-
Neuromelanin										
RBD	9/2	67±7	-	1 (0-5)	-	-	28 (24-30)	4/7	6 (3-9)	6 (3-15)
PD	21/8	67±9	6·2±4·2	37 (11-51)	2/26/1/0	-	26 (23-30)	10/16	6 (2-14)	7 (1-19)
HC	12/5	68±7	-	-	-	-	29 (27-30)	0/10	12 (6-15)	2 (0-14)
MeNER										
RBD	14/3	66±8	-	1 (0-5)	-	-	28 (24-30)	5/12	6 (2-13)	6 (2-15)
PD	22/8	67±9	6·4±4·3	37 (11-62)	2/26/1/1	-	27 (23-30)	10/16	6 (2-14)	7 (1-19)
HC	9/2	67±6	-	-	-	-	28 (27-30)	0/10	12 (6-13)	2 (0-7)
FDOPA										
RBD	17/4	68±9	-	1 (0-5)	-	-	27 (23-30)	7/14	6 (2-13)	7 (2-15)
PD	8/2	64±9	10·6±3·2	44 (29-52)	0/5/5/0	29 (24-30)	-	1/8	7 (2-10)	-
HC	14/4	64±6	-	-	-	30 (27-30)	-	0/6	12 (6-15)	2 (0-4)

Data presented as mean±SD or median (range). Orthostatic hypotension (OH) measurements were only available for a subset of the reference subjects. [DD=disease duration of PD. H&Y=Hoehn & Yahr stage. MMSE=mini-mental state examination. MoCA=Montreal cognitive assessment. UPDRS=Unified PD Rating scale – part III.]
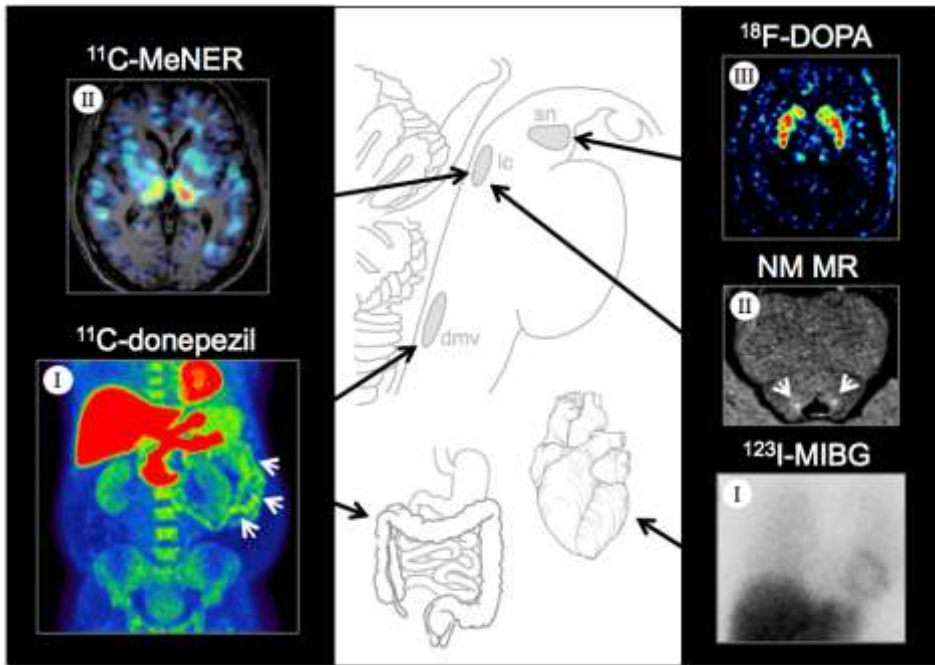
Figure 1. The five imaging modalities and their relationship to Braak stage structures involved in PD are denoted by roman numerals. **I.** ^{11}C-donepezil PET signal of the intestine is a marker of decreased acetylcholine esterase activity, reflecting cholinergic innervation including parasympathetic innervation from the dorsal motor nucleus of the vagus (DMV). Arrows indicate the small intestine. ^{123}I-MIBG is a validated tracer of sympathetic cardiac innervation **II.** ^{11}C-MeNER measures the availability of noradrenaline transporters in terminals originating from the locus coeruleus (LC). The integrity of the pigmented cell bodies of the LC is estimated by neuromelanin-sensitive MRI (arrows). **III.** Striatal dopamine storage capacity of projections from the substantia nigra (SN) is measured with ^{18}F-DOPA PET.

For the FDOPA analysis, time-activity curves were extracted from template VOIs placed in the putamen and occipital cortex. The Gjedde-Patlak graphical approach was applied to estimate specific FDOPA uptake (Ki) in putamen using occipital cortex as a reference[28]. The lowest of left/right putamen Ki values was always used for analyses. ^{11}C-MeNER uptake was investigated in the thalamus and red nucleus, since previous ^{11}C-MeNER PET studies showed robust PD vs. healthy control differences in these structures[21,22]. Template VOIs were defined in the thalamus, red nucleus, and occipital cortex (reference region), as previously described[21]. PET images were smoothed with a 4mm Gaussian filter and time activity curves extracted from VOIs for calculation of binding potentials relative to non-displaceable binding (BP_{ND}) using the simplified reference tissue model 2 (SRTM2).

Other assessments

Autonomic and non-motor symptoms were assessed with the non-motor symptoms questionnaire (NMSQuest)[29], constipation with ROME III diagnostic criteria, motor symptoms with the MDS Unified PD Rating Scale part III (MDS-UPDRS III), and RBD symptoms with the RBD symptom questionnaire[30]. Cognitive status of iRBD patients was evaluated with the MoCA battery, whereas some of the control and PD comparator groups had been assessed with the Mini mental state examination (MMSE). After 15 minutes of supine rest, blood pressure was measured for three consecutive minutes after tilting. Orthostatic hypotension was defined as systolic pressure drop of 20 mmHg or diastolic pressure drop of 10 mmHg. Olfaction was tested with the 16-item Sniffin' Sticks identification battery.

Statistical analyses

Statistical analyses were performed with Stata 14·2 and Graphpad PRISM 6. Normality of data was assessed with Shapiro-Wilk tests and Q-Q plots. Data are presented as mean±SD or median (range). Grubbs' test was used to identify statistical outliers. Demographic and clinical data were interrogated using ANOVA, Kruskal-Wallis, and chi-squared tests as appropriate. Group comparisons of imaging data were performed with one-way ANOVA. The iRBD group was subsequently compared to the control and PD groups applying Dunnett's correction for multiple comparisons. Associations between imaging data and clinical data were investigated with Pearson correlation or Spearman Rank correlation for continuous and categorical data. Significance level was set at $p < 0.05$.

Pathology index

To assess the degree to which iRBD subjects had reached "fully developed PD-level pathology" within each neuronal system, we converted the iRBD imaging data to a "PD pathology index", by defining the corresponding healthy control mean as 0% and the PD mean as 100%. Resulting pathology indices were compared to published data from previous ^{123}I-MIBG studies[19,31] and ^{123}I-FP-CIT dopamine transporter studies of iRBD patients[32,33], where controls and PD patient comparator data were presented.

Results

Clinical and demographic data

The iRBD group was 6 years older than the PD comparator group for ^{11}C-donepezil PET (p=0·04), and the male/female ratio across the three ^{123}I-MIBG subject groups was unmatched (p=0·059). There were no other significant differences in age or sex-distribution between the iRBD and comparator PD and control groups. Self-reported duration of RBD symptoms in the iRBD group was 6·3±5·6 years. The iRBD patients showed similar rates of hyposmia, orthostatic hypotension, and non-motor symptoms compared to all PD reference groups. Twenty of 22 (91%) iRBD patients were hyposmic. Two iRBD cases had MoCA scores of 23 and 24, while the remaining 20 subjects fell in the 25-30 range. These data are summarized in **Table 1**.

Imaging data

Images from the five modalities are presented in **Figure 2**. Due to logistical challenges and technical failures, there were a few missing scans in the study. All 22 iRBD patients underwent MIBG scintigraphy, 21 had FDOPA PET, 20 donepezil PET, and 17 MeNER PET. Only 11 iRBD patients had neuromelanin-sensitive MRI. See **Table 1** for exact numbers of subjects within each imaging modality. The median time lag from the first to last imaging session in the iRBD cohort was 92 days (range 7-265).

^{11}C-donepezil PET. Significant between-group differences in ^{11}C-donepezil uptake were seen in the small intestine (p=0·004, ANOVA, **Figure 3A**), and the colon (p=0·004, ANOVA, **Figure 3B**). Compared to healthy controls, iRBD patients displayed significantly lower uptake in the small intestine (p=0·0018) and colon (p=0·0020). Mean small intestine and colon values in the iRBD group were similar to PD patients (small intestine p=0·348, colon p=0·388). There was no

11

significant correlation between colon ^{11}C-donepezil SUV and severity of constipation ROME (questions 9-15) ratings (p=0·42).
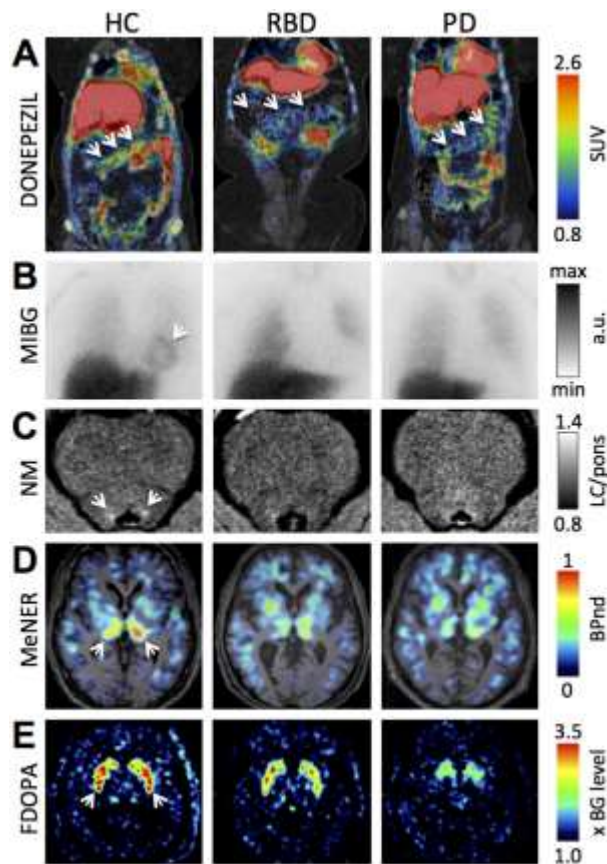

Figure 2. Representative images from healthy controls (HC), iRBD, and PD patients with the five imaging modalities. Individual cases are representative of the group mean within the respective groups. **A.** ^{11}C-donepezil PET/CT. Note lower donepezil uptake in the colon in iRBD and PD. Arrows denote transverse colon. **B.** ^{123}I-MIBG scintigraphy of the heart (arrow). Note completely absent heart uptake in iRBD and PD. **C.** Neuromelanin (NM) MRI of locus coeruleus (arrows). Note lower locus coeruleus signal in iRBD and PD. **D.** ^{11}C-MeNER PET. Thalamic MeNER binding potential (BP$_{ND}$), shown by arrows, is decreased in iRBD and PD. **E.** ^{18}F-DOPA PET. Putamen FDOPA signal (arrows) is mildly decreased in some iRBD cases, but markedly decreased in PD.

^{123}I-MIBG scintigraphy. Highly significant between-group differences were seen in the late-image mean H/M ratios (p<0·0001, ANOVA, **Figure 3C**) and also in the MIBG WR (p<0·0001, ANOVA, **Figure 3D**). Compared to controls, the iRBD group showed significantly lower H/M ratios (p<0·0001) and WR (p<0·0001). No mean difference was seen between the iRBD and PD

groups (p>0·21). Using a cut-off criterion of ">2 SD below control mean" to define a pathological MIBG scan, 18 of 22 (82%) iRBD patients had pathological H/M ratios, and 20 of 22 (91%) iRBD had pathological WR rates. No significant correlations were seen between systolic or diastolic blood pressure drop and the H/M ratios or WR values (p>0·25).
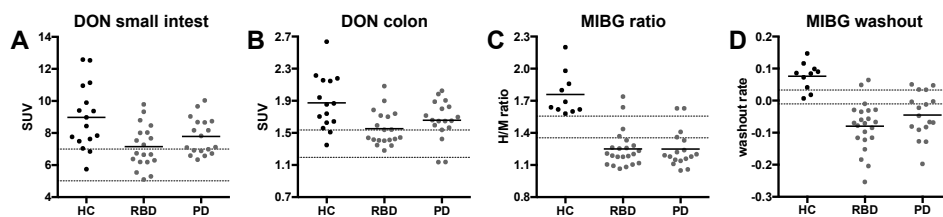

Figure 3. A-B. The volume-corrected ^{11}C-donepezil standard uptake values (SUV) in the small intestine (**A**) and colon (**B**) of healthy controls (HC), iRBD, and PD patients. The colon was impossible to define in one HC, leaving only 15 HC with colon values. **C.** Heart/mediastinum (H/M) ratio on the late ^{123}I-MIBG images. **D.** Wash out values of MIBG from the early (15 min) to late image (3·5 h). [Solid lines denote group means. Dotted lines denote -1 and -2 SD below control mean].
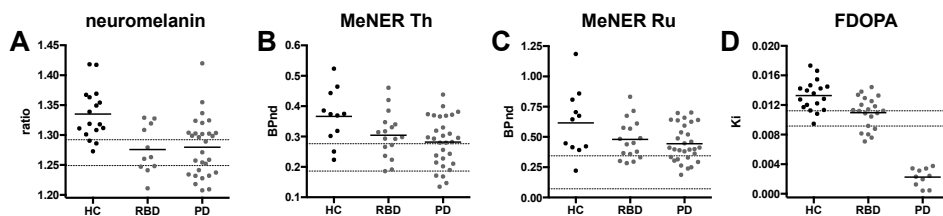

Figure 4. A. The MRI neuromelanin LC/pons ratio in healthy controls (HC), iRBD, and PD patients. **B-C.** The ^{11}C-MeNER PET binding potential (BP_{ND}) in the thalamus (Th) and nucleus ruber (Ru). **C.** The minimum (left or right) ^{18}F-DOPA Ki value in the putamen. [Solid lines denote group means. Dotted lines denote -1 and -2 SD below control mean].

Neuromelanin MRI. Highly significant differences were seen between the groups in neuromelanin LC/pons ratios (p=0·0004, ANOVA, **Figure 4A**). iRBD patients displayed significantly lower LC/pons ratios compared to the controls (p=0·0028) but similar to those of PD patients (p=0·96).

^{11}C-MeNER PET. An overall difference in thalamic ^{11}C-MeNER BP_{ND} was seen across the groups with reduced mean uptake evident in both iRBD and PD groups (p=0·017, ANOVA, **Figure 4B**). No significant differences were seen when comparing mean BP_{ND} in the iRBD group directly with the healthy controls (p=0·095) or PD patients (p=0·56). A *post hoc* analysis of the left and right BP_{ND} values individually disclosed a significant reduction in the left thalamic ^{11}C-MeNER in the iRBD group compared to controls (p=0·023, **Supplementary Figure 1**). The ^{11}C-MeNER BP_{ND} of the red nucleus also differed significantly across the three groups with reductions evident in iRBD and PD (p=0·033, ANOVA, **Figure 4C**), but no significant differences were seen when comparing the iRBD group with the healthy controls (p=0·103) or PD patients (p=0·74).

^{18}F-DOPA PET. Highly significant between-group differences were seen in putamen FDOPA Ki values (p<0·0001, ANOVA; **Figure 4D**). When using a ">2 SD below control mean" criterion of pathology, 6 of 21 (29%) iRBD patients had pathologically reduced putamen FDOPA uptake. In contrast, all PD patients had pathological FDOPA PET, and a highly significant difference was seen in mean FDOPA Ki values between iRBD and PD groups (p<0.0001).
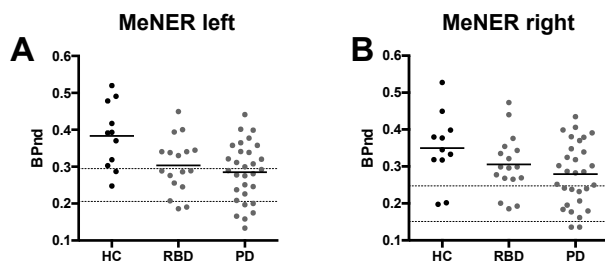
Supplementary Figure 1. The ^{11}C-MeNER PET binding potential (BP_{ND}) in the left (**A**) and right (**B**) thalamus of healthy controls (HC), iRBD, and PD patients. An overall difference in thalamic ^{11}C-MeNER BP_{ND} was seen between the groups in the left thalamus (p=0·004, **A**), and post-ANOVA comparison of the iRBD to control group showed that the ^{11}C-MeNER BP_{ND} reduction was significant in the left thalamus (p=0·023). Dotted lines denote -1 and -2 SD below control mean.

Pathology index

Figure 5 depicts the pathology indices across the five imaging modalities. iRBD patients exhibited dysfunction equivalent to PD patients on ^{11}C-donepezil PET, ^{123}I-MIBG scintigraphy, and neuromelanin MRI measures. The index for thalamic noradrenergic transporter availability

14

with ^{11}C-MeNER data was 73% but only 21% for putamen dopamine storage capacity measured with ^{18}F-DOPA PET. Pathology indices from previous ^{123}I-MIBG and dopamine transporter SPECT studies are shown for comparison (depicted with grey circles in **Figure 5**)[19,31-33]. Importantly, the iRBD patients showed extreme denervation of both the sympathetic and parasympathetic nervous systems (i.e. pathology indices >100%) compared to groups of mixed RBD-positive/negative early-stage PD patients. In contrast, the pathology indices of presynaptic dopaminergic imaging markers were 21-36%. More details are available in **Supplementary table 2.**
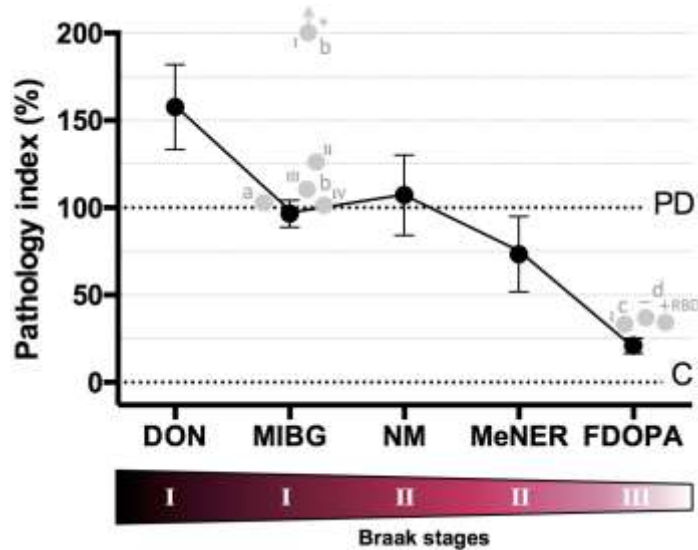

Figure 5. The figure shows pathology indices (mean±SEM) of the present iRBD imaging data (black circles) listed according to PD Braak stage structures. For each imaging modality the healthy control (C) average is set at 0% and PD average at 100%. Grey circles show pathology indices from two previous MIBG studies[19,31] (a & b), and two dopamine transporter SPECT studies[32,33] (c & d). The four grey points in b show the MIBG pathology index of iRBD patients compared to H&Y stage I through IV PD patients (roman numerals: I, II, III, IV). Note that the H&Y I index was actually 300% (denoted by * and up-arrow). That particular MIBG study demonstrated that iRBD patients show more severe cardiac sympathetic denervation than H&Y I-II PD patients (MIBG index >100%). Similarly, our iRBD group showed a donepezil PET index of 157% when compared to our early stage PD patients. In one dopamine transporter SPECT studies, iRBD patients were compared to *de novo* H&Y I patients (c), and in another iRBD cases were compared to PD patients with and without RBD (depicted with + and - RBD). [DON: donepezil colon values, NM: neuromelanin MRI]

Discussion

The "peripheral-onset" of PD hypothesis posits that formation of abnormal α-syn aggregates first occurs in nerve terminals of the olfactory, enteric, and autonomic nervous system. The aggregates then spread by retrograde axonal transport to the medullary DMV and spinal IML[3]. Here, we have demonstrated peripheral dysfunction at a level seen in established PD level in our iRBD patients who are likely to represent prodromal PD or DLB. Our findings do not prove that α-syn misfolding is initiated peripherally by neurotropic pathogens, but are compatible with this view. Our findings argue against an isolated olfactory entry site of pathogens in PD[11,34] as this would be difficult to reconcile with our observed cardiac and intestinal dysfunction and concomitant sparing of the nigra in iRBD.

[11]C-donepezil PET is not a specific marker of parasympathetic innervation, but measures acetylcholinesterase activity in both enteric neurons and parasympathetic synapses. However, pathology studies have not shown an appreciable loss of enteric neurons in PD, whereas damage to the DMV and parasympathetic sacral plexus is common. The most parsimonious explanation of decreased gastrointestinal ^{11}C-donepezil signal is, therefore, loss of parasympathetic cholinergic terminals[18]. Whatever is responsible for the reduced ^{11}C-donepezil signal in iRBD, this pathology appears to be fully developed by the prodromal stage of PD with RBD.

Nearly all our iRBD patients had pathological MIBG heart scans, in accordance with two previous, smaller iRBD studies[19,31]. Taken together, the available data show that approximately 90% of iRBD patients have profound cardiac sympathetic denervation. We saw no correlations between MIBG signals and severity of orthostatic hypotension in iRBD; this is also the case in PD[35]. Interestingly, 40-50% of H&Y stage I PD patients have normal MIBG scans, but by stage H&Y III nearly all have pathological MIBG[31]. In the light of our MIBG results in iRBD, it is possible that those early-stage PD patients with normal MIBG scans are predominantly RBD-negative[36,37]. We propose that the prodromal RBD phenotype of PD is characterized by early, severe pathology in the autonomic nervous system whereas RBD-negative early PD patients are less susceptible. This interpretation is supported by a previous MIBG report, which compared iRBD to PD patients across H&Y stages I through V[31]. These authors found MIBG pathology indices in iRBD of 300% (compared to H&Y I PD), 127% (H&Y II), 110% (H&Y III), and 102% (H&Y IV) (grey inserts in **Figure 5**).

16

The iRBD group displayed a similar reduction in LC neuromelanin signal to our diagnosed PD patients. The PD comparator group comprised 15 polysomnography-verified RBD-positive and 14 RBD-negative patients[21]. Our iRBD patients displayed a larger mean reduction in LC neuromelanin signal than the RBD-negative PD sub-group, although the difference was non-significant (**Supplementary Figure 2**)[21]. These observations are in line with previous studies of iRBD and PD[20,38] and reinforce the conclusion that iRBD patients exhibit a more profound loss of LC neuromelanin than diagnosed PD patients without RBD. Damage to pontine nuclei, including sublaterodorsal nucleus and peri-coeruleus complex, is thought to be responsible for generating the RBD phenotype[14].
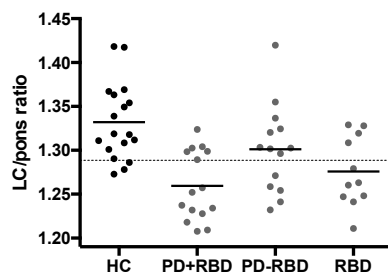
Supplementary Figure 2. The MRI neuromelanin LC/pons ratio in healthy controls (HC), iRBD, and PD patients with and without RBD. No significant differences were seen between iRBD and either PD group (iRBD vs. PD-RBD: p=0·344, iRBD vs. PD+RBD: p=0·662). However, the iRBD group displayed significantly lower values than the HC group (p=0·004). [Dotted line denotes 1 SD below control mean].

[11]C-MeNER is a reboxetine analogue that binds specifically to noradrenaline transporters. Two recent studies have reported reduced ^{11}C-MeNER binding in the red nucleus and thalamus of PD patients compared to controls[21,22]. Our iRBD patients had lower mean ^{11}C-MeNER binding bilaterally in the thalamus and red nucleus than healthy controls but the reduction only reached significance in the left thalamus after a *post hoc* analysis (**Supplementary Figure 1**). Sommerauer et al. have previously reported that RBD-positive PD patients showed significant reductions in thalamic ^{11}C-MeNER BP_{ND}, whereas RBD-negative PD patients did not. Our findings suggest that noradrenergic terminal loss is less pronounced in iRBD compared to PD patients with RBD. [11]C-

MeNER gives a low specific signal, so our study may well have lacked the power to detect bilaterally significant thalamic ^{11}C-MeNER reductions with this intrinsically noisy tracer.

29% of our iRBD patients exhibited decreased putaminal FDOPA uptake in line with previous dopamine transporter imaging studies[39,40]. Our PD comparator group for FDOPA had established disability (**Table 1**) so severe nigrostriatal dopaminergic deficits would be expected (**Figure 4D**). The use of this PD group as a comparator resulted in a low FDOPA pathology index for the iRBD patients (21%) which could have been higher if iRBD had been compared with newly diagnosed PD cases. FDOPA PET is a marker of aromatic L-amino acid decarboxylase and this becomes up-regulated in remaining terminals during the early stages of nigrostriatal degeneration[41]. Such upregulation could mask early dopaminergic dysfunction in iRBD when FDOPA PET is used as an imaging biomarker. Nevertheless, normal presynaptic dopamine imaging is considered an exclusion criterion for a PD diagnosis[24]. Since 71% of our iRBD subjects had normal putamen FDOPA uptake, we conclude that the dopaminergic system is considerably less affected in iRBD compared to the dusfunction of the autonomic nervous system and the LC.

We emphasize that our iRBD findings may only represent a valid prodrome of PD patients with additional RBD. It is accepted that RBD is associated with a more aggressive PD phenotype which shows more widespread α-syn deposition affecting most brain regions[42], and faster progression of motor and non-motor symptoms[43]. We have demonstrated that the level of dysfunction in the autonomic nervous system of iRBD patients equals, and at times exceeds, that seen in unselected PD patients. Based on its pattern of autonomic and LC involvement, we hypothesize that non-cognitively impaired iRBD parallels the Braak stage 2 PD distribution of Lewy pathology[2]. We speculate that this supports the view that, during the prodromal phase of PD or DLB with RBD, the α-syn pathology responsible originates in peripheral autonomic/enteric nerve terminals. In contrast, RBD-negative early-stage PD patients may have a more benign phenotype where α-syn pathology is primarily initiated within the CNS and olfactory bulb. This hypothesis is speculative, but would explain why not all PD patients show a Braak-like distribution of α-syn pathology at post-mortem - 20% of cases have no pathology in the DMV[11].

The dual-hit hypothesis is based on post-mortem Braak staging of PD brains[2], however, DLB cases can exhibit alternative distributions of α-syn pathology[44]. Our choice to study iRBD as a prodrome of PD can be criticized as ~50% of iRBD subjects will convert to DLB[12,13]. Despite this

caveat, our findings strongly suggest that iRBD represents a prodrome of both DLB and PD with RBD and these patients are similar with respect to having early peripheral autonomic and LC dysfunction. We will follow-up our iRBD cases to determine whether those patients with a final PD+RBD diagnosis show more extensive peripheral dysfunction than the DLB converters. Finally, we propose that MIBG scintigraphy may be useful for predicting which iRBD cases will progress to clinical MSA as cardiac sympathetic innervation is preserved in this synucleinopathy[35]. We speculate that those iRBD cases with normal MIBG scans have a higher probability of representing prodromal MSA. This assertion needs confirmation in future studies.

The pattern of neuronal cell loss seen in PD does not parallel the severity of Lewy pathology and it has been suggested that regional or cell-related factors could be responsible for this[9,11]. Our findings are relevant to this discussion, since we primarily used markers of nerve terminal function, not cell body loss. α-syn is a synaptic protein and its initial aggregation is thought to take place in neuronal terminals[1]. Studies have shown a more dramatic loss of nerve terminals compared to cell bodies across several neurotransmitter systems in PD[35,45]. This implies that neurons containing Lewy pathology will be most dysfunctional at a synaptic level, while their cell bodies may remain intact. Our results in iRBD show a pattern of neuronal terminal damage that parallels Braak stage 2 of Lewy body pathology although cell body loss measured in post-mortem studies of early PD patients does not follow Braak α-syn staging. The fact that some neurons containing α-syn aggregates are more resistant to apoptosis than others is not against the hypothesis that α-syn aggregates can be transmitted through inter-connected neuronal networks, nor that the initial α-syn aggregation may first occur in peripheral nerve terminals in some individuals.

This study has several limitations: First, we used different groups of healthy controls and PD patients as comparators when analysing iRBD imaging findings. This was to limit levels of radiation exposure to healthy and PD subjects and maintain scan tolerance as far as possible in our complex PET/MRI programme. However, except for minor differences in age distribution of the ^{11}C-donepezil groups and an unmatched male/female ratio in the ^{123}I-MIBG data, all HC and PD reference groups were reasonably comparable to the iRBD patients in terms of demographic findings. Second, we included both early-stage and later-stage PD comparator groups. Thus, our pathology index of iRBD relative to PD for different imaging biomarkers (**Figure 5**) must be interpreted with caution. The most important finding is that the iRBD cases showed peripheral cholinergic and noradrenergic dysfunction and LC melanin loss at a similar level to diagnosed PD

19

patients. Third, our iRBD sample size of 22 was modest affecting our power to interrogate data statistically, particularly the neuromelanin and ^{11}C-MeNER analyses. These cases, however, are not easy to find and recruit for complex imaging programmes. Fourth, since ^{11}C-donepezil PET is not a specific parasympathetic marker, the significant intestinal ^{11}C-donepezil signal reductions in iRBD may indicate both parasympathetic and local enteric nerve terminal damage.

In conclusion, iRBD patients display neuronal dysfunction in the peripheral autonomic nervous system and locus coeruleus equivalent to diagnosed PD patients although 71% of these iRBD patients have normal nigrostrial dopaminergic innervation. This pattern of dysfunction parallels Braak stage 2 α-syn pathology in PD and supports the hypothesis that α-syn misfolding and aggregation in iRBD, a prodrome of both PD and DLB with RBD, initially targets terminals of the peripheral nervous system.

Contributors

PB and DJB designed the study. KK, TDF, CPB, MO, and KBS recruited iRBD subjects. KK, TDF, AKH, MS, AN, MGS, NP, and PB performed imaging and statistical data analyses. All authors contributed to data analyses and writing of the manuscript.

Acknowledgments

Competing financial interests.

The authors declare no competing financial interests.

References

1.   Uchihara T, Giasson BI. Propagation of alpha-synuclein pathology: hypotheses, discoveries, and yet unresolved questions from experimental and human brain studies. *Acta Neuropathol* 2016; **131**(1): 49-73.

2.   Braak H, Del Tredici K, Rub U, de Vos RA, Jansen Steur EN, Braak E. Staging of brain pathology related to sporadic Parkinson's disease. *Neurobiol Aging* 2003; **24**(2): 197-211.

3.   Braak H, Rub U, Gai WP, Del Tredici K. Idiopathic Parkinson's disease: possible routes by which vulnerable neuronal types may be subject to neuroinvasion by an unknown pathogen. *J Neural Transm (Vienna)* 2003; **110**(5): 517-36.

4.   Borghammer P. How does parkinson's disease begin? Perspectives on neuroanatomical pathways, prions, and histology. *Mov Disord* 2017.

5.   Pan-Montojo F, Anichtchik O, Dening Y, et al. Progression of Parkinson's disease pathology is reproduced by intragastric administration of rotenone in mice. *PLoS One* 2010; **5**(1): e8762.

6.   Svensson E, Horvath-Puho E, Thomsen RW, et al. Vagotomy and subsequent risk of Parkinson's disease. *Ann Neurol* 2015; **78**(4): 522-9.

7.   Liu B, Fang F, Pedersen NL, et al. Vagotomy and Parkinson disease: A Swedish register-based matched-cohort study. *Neurology* 2017.

8.   Stokholm MG, Danielsen EH, Hamilton-Dutoit SJ, Borghammer P. Pathological alpha-synuclein in gastrointestinal tissues from prodromal Parkinson disease patients. *Ann Neurol* 2016; **79**(6): 940-9.

9.   Lionnet A, Leclair-Visonneau L, Neunlist M, et al. Does Parkinson's disease start in the gut? *Acta Neuropathol* 2017.

10.   Brundin P, Melki R. Prying into the Prion Hypothesis for Parkinson's Disease. *J Neurosci* 2017; **37**(41): 9808-18.

11.   Surmeier DJ, Obeso JA, Halliday GM. Parkinson's Disease Is Not Simply a Prion Disorder. *J Neurosci* 2017; **37**(41): 9799-807.

12.   Iranzo A, Tolosa E, Gelpi E, et al. Neurodegenerative disease status and post-mortem pathology in idiopathic rapid-eye-movement sleep behaviour disorder: an observational cohort study. *Lancet neurology* 2013; **12**(5): 443-53.

13.   Postuma RB, Gagnon JF, Bertrand JA, Genier Marchand D, Montplaisir JY. Parkinson risk in idiopathic REM sleep behavior disorder: preparing for neuroprotective trials. *Neurology* 2015; **84**(11): 1104-13.

14.   Boeve BF. Idiopathic REM sleep behaviour disorder in the development of Parkinson's disease. *Lancet neurology* 2013; **12**(5): 469-82.

21

15.   Sprenger FS, Stefanova N, Gelpi E, et al. Enteric nervous system alpha-synuclein immunoreactivity in idiopathic REM sleep behavior disorder. *Neurology* 2015; **85**(20): 1761-8.

16.   Iranzo A, Gelpi E, Tolosa E, et al. Neuropathology of prodromal Lewy body disease. *Mov Disord* 2014; **29**(3): 410-5.

17.   Fedorova TD, Seidelin LB, Knudsen K, et al. Decreased intestinal acetylcholinesterase in early Parkinson disease: An 11C-donepezil PET study. *Neurology* 2017; **88**(8): 775-81.

18.   Gjerloff T, Fedorova T, Knudsen K, et al. Imaging acetylcholinesterase density in peripheral organs in Parkinson's disease with 11C-donepezil PET. *Brain* 2015; **138**(Pt 3): 653-63.

19.   Miyamoto T, Miyamoto M, Inoue Y, Usui Y, Suzuki K, Hirata K. Reduced cardiac 123I-MIBG scintigraphy in idiopathic REM sleep behavior disorder. *Neurology* 2006; **67**(12): 2236-8.

20.   Ehrminger M, Latimier A, Pyatigorskaya N, et al. The coeruleus/subcoeruleus complex in idiopathic rapid eye movement sleep behaviour disorder. *Brain* 2016; **139**(Pt 4): 1180-8.

21.   Sommerauer M, Fedorova T, Hansen AK, et al. Evaluation of the noradrenergic system in Parkinson's disease - An 11C-MeNER PET and neuromelanin MRI study. *Brain* 2017; **in press**.

22.   Nahimi A, Sommerauer M, Kinnerup MB, et al. Noradrenergic deficits in Parkinson's disease imaged with 11C-MeNER. *J Nucl Med* 2017.

23.   Stokholm MG, Iranzo A, Ostergaard K, et al. Assessment of neuroinflammation in patients with idiopathic rapid-eye-movement sleep behaviour disorder: a case-control study. *Lancet neurology* 2017; **16**(10): 789-96.

24.   Postuma RB, Berg D, Stern M, et al. MDS clinical diagnostic criteria for Parkinson's disease. *Mov Disord* 2015; **30**(12): 1591-601.

25.   McKeith IG, Boeve BF, Dickson DW, et al. Diagnosis and management of dementia with Lewy bodies: Fourth consensus report of the DLB Consortium. *Neurology* 2017; **89**(1): 88-100.

26.   Bloch A, Probst A, Bissig H, Adams H, Tolnay M. Alpha-synuclein pathology of the spinal and peripheral autonomic nervous system in neurologically unimpaired elderly subjects. *Neuropathol Appl Neurobiol* 2006; **32**(3): 284-95.

27.   Dickson DW, Fujishiro H, DelleDonne A, et al. Evidence that incidental Lewy body disease is pre-symptomatic Parkinson's disease. *Acta Neuropathol* 2008; **115**(4): 437-44.

28.   Moore RY, Whone AL, McGowan S, Brooks DJ. Monoamine neuron innervation of the normal human brain: an 18F-DOPA PET study. *Brain Res* 2003; **982**(2): 137-45.

29.   Chaudhuri KR, Martinez-Martin P, Schapira AH, et al. International multicenter pilot study of the first comprehensive self-completed nonmotor symptoms questionnaire for Parkinson's disease: the NMSQuest study. *Mov Disord* 2006; **21**(7): 916-23.

30.   Stiasny-Kolster K, Mayer G, Schafer S, Moller JC, Heinzel-Gutenbrunner M, Oertel WH. The REM sleep behavior disorder screening questionnaire--a new diagnostic instrument. *Mov Disord* 2007; **22**(16): 2386-93.

31.   Kashihara K, Imamura T, Shinya T. Cardiac 123I-MIBG uptake is reduced more markedly in patients with REM sleep behavior disorder than in those with early stage Parkinson's disease. *Parkinsonism Relat Disord* 2010; **16**(4): 252-5.

32.   Rolinski M, Griffanti L, Piccini P, et al. Basal ganglia dysfunction in idiopathic REM sleep behaviour disorder parallels that in early Parkinson's disease. *Brain* 2016; **139**(Pt 8): 2224-34.

33.   Zoetmulder M, Nikolic M, Biernat H, Korbo L, Friberg L, Jennum P. Increased Motor Activity During REM Sleep Is Linked with Dopamine Function in Idiopathic REM Sleep Behavior Disorder and Parkinson Disease. *J Clin Sleep Med* 2016; **12**(6): 895-903.

34.   Adler CH, Beach TG. Neuropathological basis of nonmotor manifestations of Parkinson's disease. *Mov Disord* 2016; **31**(8): 1114-9.

35.   Orimo S, Yogo M, Nakamura T, Suzuki M, Watanabe H. Brain imaging in Aging Special Issue of Ageing Research Reviews I-meta-iodobenzylguanidine (MIBG) cardiac scintigraphy in alpha-synucleinopathies. *Ageing research reviews* 2016.

36.   Nomura T, Inoue Y, Hogl B, et al. Relationship between (123)I-MIBG scintigrams and REM sleep behavior disorder in Parkinson's disease. *Parkinsonism Relat Disord* 2010; **16**(10): 683-5.

37.   Kim JS, Park HE, Oh YS, et al. Orthostatic hypotension and cardiac sympathetic denervation in Parkinson disease patients with REM sleep behavioral disorder. *J Neurol Sci* 2016; **362**: 59-63.

38.   Garcia-Lorenzo D, Longo-Dos Santos C, Ewenczyk C, et al. The coeruleus/subcoeruleus complex in rapid eye movement sleep behaviour disorders in Parkinson's disease. *Brain* 2013; **136**(Pt 7): 2120-9.

39.   Iranzo A, Valldeoriola F, Lomena F, et al. Serial dopamine transporter imaging of nigrostriatal function in patients with idiopathic rapid-eye-movement sleep behaviour disorder: a prospective study. *Lancet neurology* 2011; **10**(9): 797-805.

40.   Meles SK, Vadasz D, Renken RJ, et al. FDG PET, dopamine transporter SPECT, and olfaction: Combining biomarkers in REM sleep behavior disorder. *Mov Disord* 2017; **32**(10): 1482-6.

41.   Lee CS, Samii A, Sossi V, et al. In vivo positron emission tomographic evidence for compensatory changes in presynaptic dopaminergic nerve terminals in Parkinson's disease. *Ann Neurol* 2000; **47**(4): 493-503.

42.   Postuma RB, Adler CH, Dugger BN, et al. REM sleep behavior disorder and neuropathology in Parkinson's disease. *Mov Disord* 2015; **30**(10): 1413-7.

43.   Fereshtehnejad SM, Romenets SR, Anang JB, Latreille V, Gagnon JF, Postuma RB. New Clinical Subtypes of Parkinson Disease and Their Longitudinal Progression: A Prospective Cohort Comparison With Other Phenotypes. *JAMA Neurol* 2015; **72**(8): 863-73.

44.   Beach TG, Adler CH, Lue L, et al. Unified staging system for Lewy body disorders: correlation with nigrostriatal degeneration, cognitive impairment and motor dysfunction. *Acta Neuropathol* 2009; **117**(6): 613-34.

45.   Colom-Cadena M, Pegueroles J, Herrmann AG, et al. Synaptic phosphorylated alpha-synuclein in dementia with Lewy bodies. *Brain* 2017; **140**(12): 3204-14.

Figure Legends

Figure 1. The five imaging modalities and their relationship to Braak stage structures are denoted by roman numerals. **I.** ^{11}C-donepezil PET signal of the intestine is a surrogate marker of decreased cholinergic innervation, including parasympathetic innervation from the dorsal motor nucleus of the vagus (DMV). Arrows indicate the small intestine. ^{123}I-MIBG is a validated tracer of sympathetic cardiac innervation **II.** ^{11}C-MeNER measures the density of noradrenergic terminals originating in the locus coeruleus (LC). The integrity of the pigmented cell bodies of the LC is estimated by neuromelanin-sensitive MRI (arrows). **III.** Striatal dopaminergic innervation from the substantia nigra (SN) is measured by ^{18}F-DOPA PET.

Figure 2. Representative images from healthy controls (HC), iRBD, and PD patients with the five imaging modalities. Individual cases are representative of the group mean within the respective groups. A. ^{11}C-donepezil PET/CT. Note lower donepezil uptake in the colon in iRBD and PD. Arrows denote transverse colon. B. ^{123}I-MIBG scintigraphy of the heart (arrow). Note completely absent heart uptake in iRBD and PD. C. Neuromelanin (NM) MRI of locus coeruleus (arrows). Note lower locus coeruleus signal in iRBD and PD. D. ^{11}C-MeNER PET. Thalamic MeNER binding potential (BP$_{ND}$), shown by arrows, is decreased in iRBD and PD. E. ^{18}F-DOPA PET. Putamen FDOPA signal (arrows) is mildly decreased in some iRBD cases, but markedly decreased in PD.

Figure 3. A-B. The volume-corrected ^{11}C-donepezil standard uptake values (SUV) in the small intestine (**A**) and colon (**B**) of healthy controls (HC), iRBD, and PD patients. The colon was impossible to define in one HC, leaving only 15 HC with colon values. **C.** Heart/mediastinum (H/M) ratio on the late ^{123}I-MIBG images. **D.** Wash out values of MIBG from the early (15 min) to late image (3·5 h). [Solid lines denote group means. Dotted lines denote -1 and -2 SD below control mean].

Figure 4. A. The MRI neuromelanin LC/pons ratio in healthy controls (HC), iRBD, and PD patients. **B-C.** The ^{11}C-MeNER PET binding potential (BP_{ND}) in the thalamus (Th) and nucleus ruber (Ru). **C.** The minimum (left or right) ^{18}F-DOPA Ki value in the putamen. [Solid lines denote group means. Dotted lines denote -1 and -2 SD below control mean].

Figure 5. The figure shows pathology indices (mean±SEM) of the present iRBD imaging data (black circles) listed according to Braak stage structures. For each imaging modality the healthy control (C) average is set at 0% and PD average at 100%. Grey circles show pathology indices from two previous MIBG studies[19,31] (a & b), and two dopamine transporter SPECT studies[32,33] (c & d). The four grey points in b show the MIBG pathology index of iRBD patients compared to H&Y stage I through IV PD patients (roman numerals: I, II, III, IV). Note that the H&Y I index was actually 300% (denoted by * and up-arrow). That particular MIBG study demonstrated that iRBD patients show more severe cardiac sympathetic denervation than H&Y I-II PD patients (MIBG index >100%). Similarly, our iRBD group showed a donepezil PET index of 157% when compared to our early stage PD patients. In one dopamine transporter SPECT studies, iRBD patients were compared to *de novo* H&Y I patients (c), and in another iRBD cases were compared to PD patients with and without RBD (depicted with + and - RBD). [DON: donepezil colon values, NM: neuromelanin MRI]